

Temperature dependent percolation mechanism for conductivity in $\text{Y}_{0.63}\text{Ca}_{0.37}\text{TiO}_3$ revealed by a microstructure study

R. German,¹ B. Zimmer,¹ T. C. Koethe,¹ A. Barinov,² A. C. Komarek,^{1,3} M. Braden,¹ F. Parmigiani,^{1,2,4} and P.H.M. van Loosdrecht¹

¹*II. Physikalisches Institut, Universität zu Köln, Zùlpicher Straße 77, D-50937 Köln, Germany*

²*Sincrotrone Trieste S.C.p.A., Strada Statale 14-km 163,5 in AREA Science Park, 34149 Basovizza, Trieste, Italy*

³*Max Planck Institute for Chemical Physics of Solids, Nöthnitzer Straße 40, 01187 Dresden, Germany*

⁴*Department of Physics, University of Trieste, Via A. Valerio 2, 34127 Trieste, Italy*

(Dated: May 26, 2022)

We have performed optical microscopy, micro-photoelectron spectroscopy, and micro-Raman scattering measurements on $\text{Y}_{0.63}\text{Ca}_{0.37}\text{TiO}_3$ single crystals in order to clarify the interplay between the microstructure and the temperature dependent electronic transport mechanisms in this material. Optical microscopy observations reveal dark and bright domain patterns on the surface with length scales of the order of several to a hundred micrometers showing a pronounced temperature dependent evolution. Spatially resolved photoelectron spectroscopy measurements show the different electronic character of these domains. Using micro-Raman spectroscopy, we observe a distinct temperature dependence of the crystal structure of these domains. On the basis of these findings the different domains are assigned to insulating and metallic volume fractions, respectively. By decreasing the temperature, the volume fraction of the conducting domains increases, hence allowing the electrons to percolate through the sample at temperatures lower than ~ 150 K.

Keywords: Metal-insulator transition, transition-metal compounds, percolation.

I. INTRODUCTION

In the past decades the perovskite YTiO_3 has attained much interest as a toy material for correlated electron systems due to its simple Ti-3d^1 electronic structure.[1–4] It is classified as a typical Mott-Hubbard-insulator with a Mott-Hubbard gap of ~ 1 eV and charge transfer gap of ~ 4 eV.[5–7] By substituting Y^{3+} with Ca^{2+} in $\text{Y}_{1-x}\text{Ca}_x\text{TiO}_3$, *i.e.* hole-doping, first the ferromagnetic order vanishes at $x \sim 0.15$. By further doping, the macroscopic electronic property of this material changes from insulating to metallic at $x > 0.39$. For doping between $x = 0.33$ and $x = 0.39$ these samples exhibit a peculiar temperature driven metal-insulator transition (MIT), meaning that they are conducting at low temperatures and become insulating at higher temperatures with a transition temperature ranging from ~ 90 K to ~ 220 K with increasing x . [8, 9] This is rather uncommon as mostly the insulating phase is found to be more stable at lower temperatures. The most remarkable in the doping range of $x = 0.33 - 0.39$ is the compound $\text{Y}_{0.63}\text{Ca}_{0.37}\text{TiO}_3$, which exhibits in addition a hysteresis in the electrical resistivity and the magnetic susceptibility.[10]

$\text{Y}_{0.63}\text{Ca}_{0.37}\text{TiO}_3$ undergoes a structural phase transition from high temperature orthorhombic Pbnm (HTO) to low-temperature monoclinic $\text{P2}_1/\text{n}$ (LTM) symmetry at ~ 200 K.[11] This LTM phase has been shown to be orbitally ordered, and possibly also charge ordered.[12] As seen in electrical resistivity measurements, the compound is insulating at room temperature and the MIT

for this compound takes place at ~ 150 K.[13] ¹ Thus the crystallographic transition from HTO to LTM is not related to a change in the macroscopic electronic property and the sample remains insulating in the LTM phase. Upon further cooling below 200 K, a low-temperature orthorhombic Pbnm (LTO) phase appears and starts to coexist with the LTM phase.[11] This LTO phase is distinguished from the HTO phase, as it has a smaller unit cell than the HTO phase.[12] The volume fraction of the LTO phase increases by lowering the temperature, accompanying the metal insulator transition.[13] Thus, a possible conducting character of the LTO phase would suggest a percolation mechanism underlying the MIT. The phase separation is also observed in conducting samples ($x > 0.40$), where the volume fraction of the LTO phase is high enough even at room temperature to render these samples conducting, assuming the LTO phase to be metallic.[14] In this work we will directly show the relationship of the crystallographic structure of $\text{Y}_{1-x}\text{Ca}_x\text{TiO}_3$ and its macroscopic electronic properties. For this we investigated the material $\text{Y}_{1-x}\text{Ca}_x\text{TiO}_3$ with $x = 0.37$, exhibiting the pronounced hysteresis at the MIT.[15] Optical microscopy studies allow to follow the temperature and spatial evolution of coexisting domains in this material. Using micro photoemission studies it is possible to classify the coexisting domains to conducting and insulating phases. Finally, using micro Raman studies, these coexisting domains are also classified to their crystallo-

¹ The lattice parameters and physical properties of our samples with the chemical composition $x = 37$ %, as determined experimentally (see Sec. II), correspond to samples with $x = 39$ % in ref. [13].

graphic structures, hence allowing to directly relate the microstructure to the electronic behavior of this material, underlying the temperature driven MIT.

II. EXPERIMENTAL

The untwinned single crystal $\text{Y}_{0.63}\text{Ca}_{0.37}\text{TiO}_3$ was grown by the floating-zone technique. The oxygen stoichiometry was checked by thermal gravimetric analysis (TGA) to be 3 ± 0.02 , while the Ca content was determined from a comparison of the measured lattice constants with the results of ref.[16] (see also ref.[15], figure 5.10) to be $x = 0.37 \pm 0.01$. The optical microscopy studies of the mechanically polished samples were done in the back-reflection geometry, using a microscope with an objective of 8x magnification and numerical aperture of 0.18. The photoemission microscopy was performed at the spectromicroscopy beamline operated by the Elettra storage ring.[17] Photons at 74 eV were focused through a Schwarzschild objective, to obtain a sub-micron size spot on the sample. The measurements were performed in ultra-high vacuum at a base pressure of $p < 2 \times 10^{-10}$ mbar on *insitu* cleaved (001)-surfaces. The temperature of the sample was $T = 110$ K throughout the photoemission measurements.

For the spontaneous micro-Raman setup a continuous wave DPSS laser of 532 nm wavelength was used as a light source, sent through a microscope with a long distance objective and a numerical aperture of 0.2. The Raman scattered light was collected in a back-scattering geometry using a triple subtractive spectrometer equipped with a liquid nitrogen cooled CCD camera. This setup yields an energy resolution of 7 cm^{-1} . The samples were mounted in an Oxford Microstat cryostat, cooled by liquid Helium.

In this work the following back-scattering geometry for the Raman measurements was used: the incoming laser light propagates in the c -direction of the sample and the polarization of the incident and detected scattered light were each directed in the a -direction of the sample, abbreviated in the Porto notation as $c(aa)\bar{c}$. With the microscope, the spot-size of the laser beam is $\sim 30 \mu\text{m}$ in diameter and the position of the laser spot on the sample was fixed with an accuracy of $\pm 2.5 \mu\text{m}$. The power of the incident laser light was set to 1.7 mW.

III. RESULTS AND DISCUSSION

A. Optical microscopy

The top panel of figure 1 shows microscope images of a $\text{Y}_{0.63}\text{Ca}_{0.37}\text{TiO}_3$ single crystal at $T = 10$ K in three different orientations, *i. e.* facing a (001), (010), and (100) surface of the material, respectively, with respect to the orthorhombic Pbnm symmetry. For each of these different orientations, specific patterns of bright and dark

regions appear which show a preferred direction. As a result, the whole sample surface partitions in stripe-like patterns with a width of the order of $10 - 20 \mu\text{m}$. While on the (100)-surface, these stripes extend across the whole field of view of several hundreds of μm , on the other two surfaces they form disconnected islands of one kind with extensions of the order of $100 - 200 \mu\text{m}$ within a background of the other kind. The bottom panel of figure 1 shows the evolution of the pattern with temperature from 100 K to room temperature for the (001)-surface. Comparing figure 1(a) and figure 1(d), it is seen, that islands of brighter areas exist at 10 K, which grow upon heating, while their shape is mainly maintained even at 100 K. Upon further heating a growth of these islands in a and b directions of the sample continues. However, this growth starts to take place more rapidly, so that these islands start to connect in a and b directions at ~ 140 K. Furthermore, at ~ 150 K, bright stripes evolving in b direction start to occur within the dark background. The width of these sub-stripes is $\sim 5 \mu\text{m}$ and the distance between the stripes is $\sim 20 \mu\text{m}$. Finally, the brighter areas consisting of the former islands and the evolving stripes continue to grow and form a connected network as it is shown in figure 1(e) for 170 K.

The contrast between bright and dark areas continuously weakens above 100 K and eventually becomes insignificant at room temperature. However, by artificially enhancing the contrast of the microscope images, the different areas can be shown to still exist at 296 K, as shown in figure 1(f).

A noteworthy observation is the fact that the bright areas invariably show up in the same positions after several temperature cycles. Given the exceptionally high doping level, it seems likely to assume chemical inhomogeneity of the material to be the reason for this pattern. Additionally, the microscope images show temperature hysteresis of the surface fractions in the same temperature region as reported in the resistivity data. Remarkable is, however, the unusually large length scales in the range of many tens to hundreds of μm , *i. e.* several orders of magnitude larger than what had previously been reported.[14]

B. Spatially resolved photoelectron spectroscopy

In order to investigate the electronic properties of the different areas observed in the microscope images, spatially resolved photoelectron spectroscopy measurements have been carried out at $T = 110$ K. The inset in figure 2a) shows the Ti 3d spectral weight for two different sites on the sample, denoted as 'A' and 'B'. As the blowup in the main panel reveals, the spectra especially differ in a narrow region close to the Fermi level, with 'B' being slightly more conducting than 'A'.

Figure 2b) shows a map of a $200 \mu\text{m} \times 70 \mu\text{m}$ area of the sample with a pixel size of $1 \mu\text{m}^2$. The sample surface was oriented in [001]-direction and fractured before the measurement to get a clean surface. For each pixel, a

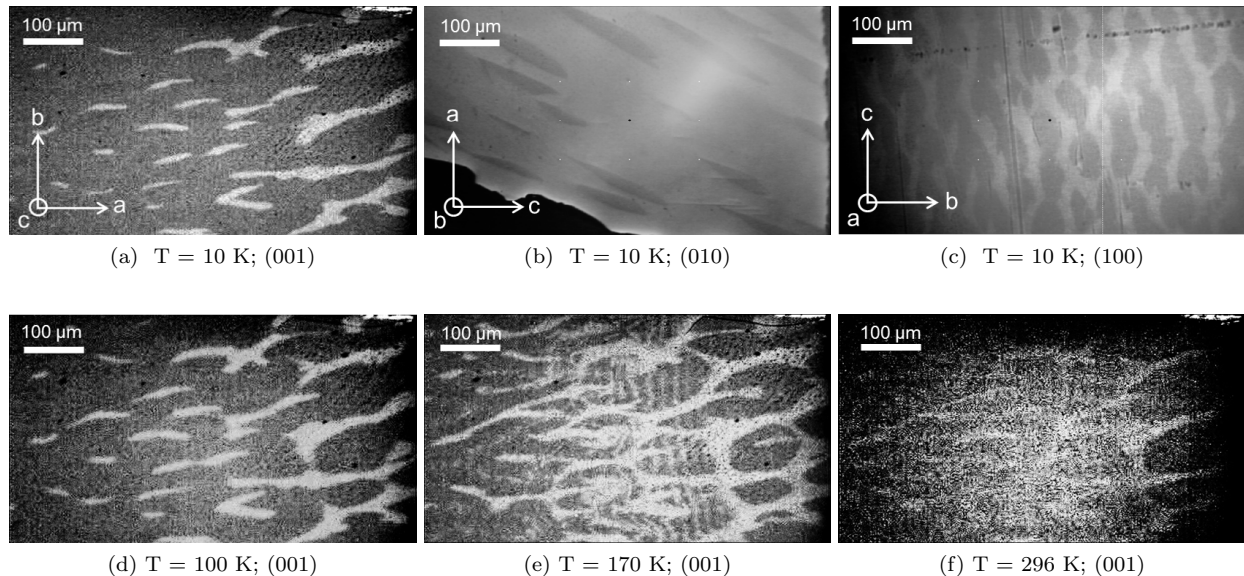


Figure 1: Microscope images of $\text{Y}_{0.63}\text{Ca}_{0.37}\text{TiO}_3$. (1a) - (1c) pattern formation for the three surface orientations, (001), (010), and (100), respectively, at 10K. (1d) - (1f) temperature evolution of the (001)-surface pattern.

full spectrum in the energy range as shown in the inset of figure 2a) has been taken. Photoemission intensity variations due to surface roughness etc. have been corrected for by normalizing each spectrum to unity. The map shows the integrated intensity in a narrow energy window around the Fermi level, *i.e.* the region where the spectra from sites 'A' and 'B' vary, as color values. Thus, more conducting regions appear bright and red in the figure in contrast to the insulating blue ones. The map reveals a similar domain pattern of stripes with a separation of $\approx 20 \mu\text{m}$ as had been observed in the microscope images. Furthermore, a smaller scale stripe formation is recognizable. The widths and distances between these sub-strips are of the order of $\sim 1 \mu\text{m}$. Stripe-like features are also observed in the photoemission spectral weights of the O $2p$ band which is a natural consequence of the hybridization with the Ti $3d$, and presumably related to a rigid band shift. The presumption based on the microscope observations, that the origin of the stripe pattern might be chemical inhomogeneity, appears to be in line with the results of the photoelectron spectroscopy.

C. Spontaneous micro-Raman spectroscopy

Various Raman investigations on $\text{Y}_{1-x}\text{Ca}_x\text{TiO}_3$ are available in the literature, showing that the Raman spectra are quite different between insulating ($x < 0.33$) and metallic ($x > 0.39$) samples at low temperatures.[18, 19] However, the phonon energies at room temperature do not change significantly by doping. This suggests, that mode assignments on YTiO_3 can be transferred to our doped material.[19] Phonon mode calculations

are available for the perovskitelike YMnO_3 . [20] As the $\text{Ti}^{3+}/\text{Mn}^{3+}$ ions do not participate in the Raman active modes, no significant shift in the mode energies due to their different masses are expected. Table I shows the phonon energies for YMnO_3 , both lattice dynamical calculations (LDC) and experimentally observed values compared to the experimentally obtained values for YTiO_3 . [19] This shows that there is indeed a good overall agreement in energies of both materials. Finally, the Raman shifts of $\text{Y}_{0.63}\text{Ca}_{0.37}\text{TiO}_3$ obtained in this work from fits of the Raman spectra are also listed in Tab. I. This comparison allows an explicit mode assignment of the observed phonon peaks. The Raman active modes for $\text{Y}_{0.63}\text{Ca}_{0.37}\text{TiO}_3$ in Pbnm symmetry are assumed to be $\Gamma = 7A_g + 5B_{1g} + 7B_{2g} + 5B_{3g}$. The Wyckoff positions are 4(c) for both Y and O1, 4(a) for Ti, and 8(d) for O2. But only Y, O1 and O2 yield Raman active modes. The Raman scattered light corresponding to A_g -modes retains the polarization of the incoming light, referred to in experiment as *parallel polarization*, while for the B_{1g} -, B_{2g} -, and B_{3g} -modes, the polarization changes with the Raman process, thus these are observed in *cross polarized* geometry. The phase transition from Pbnm to $\text{P2}_1/\text{n}$ preserves the total number of modes, because the primitive cell is the same in both phases and inversion symmetry is not broken. However, this transition leads to a redistribution of orthorhombic B_g -modes to monoclinic A_g ones. Therefore, the polarization dependence of the Raman modes can be used to identify the crystallographic phase of the material. Figure 3a) shows the Raman spectra in $c(\text{aa})\bar{c}$ geometry at 10 K, obtained from two different spots on the sample, corresponding to distinct phases, as described above in the optical mi-

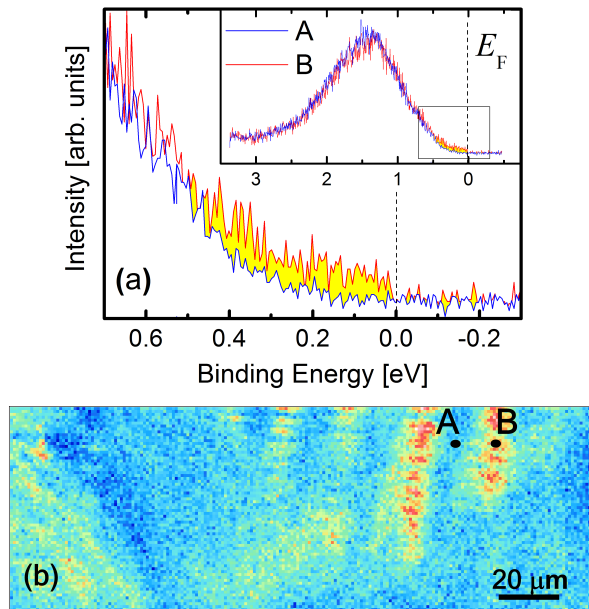


Figure 2: (Color online) Spatially resolved photoemission spectra of the Ti 3d band at 110K with sample orientation in [001]-direction. (a) Comparison between conducting and insulating spectrum in red and blue, respectively, at two different spots on the sample, denoted as 'A' and 'B'. (b) $200\ \mu\text{m} \times 70\ \mu\text{m}$ cut-out of the spatially resolved and normalized Ti 3d band photoemission spectra. Side 'A' and 'B' are indicated by black dots.

crosscopy section. Significant differences are visible in the spectral weights and peak positions of the Raman spectra obtained from the bright and dark phases, respectively, see Fig.1a. The energy regions at ~ 310 , ~ 390 and $\sim 640\ \text{cm}^{-1}$, denoted as P1, P2, and P3, respectively, exhibit the most prominent differences between the two phases. As reported in Tsurui *et al.* (2004),[19] the modes P1 and P2 are fingerprints of Raman spectra obtained from conducting samples with doping level $x > 0.39$, while P3 is only visible for doping levels $x < 0.39$, thus belonging to the insulating phase. Therefore, the Raman spectra allow us to identify the darker areas of the sample in Fig. 1a, as the LTO phase, represented by P1 and P2, and the brighter areas as the LTM phase, represented by P3. Figure 3b) and c) show the temperature dependence of the spectra for spatially fixed positions in conducting and insulating regions, respectively, in the range from 10 K to room temperature. Of particular interest is the feature P3, which is strongest in the insulating domain at 10 K. The polarization geometry and the calculated frequencies from the literature suggest that the feature consists of the $B_{2g}(1)$ breathing mode and of other bond-stretching modes. These become Raman active in parallel polarization in the monoclinic phase and show a strong temperature dependence. Note, that the structural distortions,

Mode	YMnO ₃	YMnO ₃	YTiO ₃	Y _{0.63} Ca _{0.37} TiO ₃
	Calc.	Exp.	Exp.	LTM - phase
$A_g(7)$	104	151	145	
$A_g(5)$	147	188	168	
$A_g(2)$	223	288	273	
$A_g(6)$	304	323	314	294
$A_g(4)$	407	396	417	394
$A_g(3)$	466	497	446	457
$A_g(1)$	524	518	512	532
$B_{1g}(7)$	137	151	142	
$B_{1g}(5)$	162	220	219	
$B_{1g}(4)$	285	317	306	
$B_{1g}(6)$	393	341	328	
$B_{1g}(3)$	470	481	487	
$B_{1g}(2)$	583	537	521	
$B_{1g}(1)$	617	616	643	
$B_{2g}(5)$	145	178	151	
$B_{2g}(4)$	363	336	284	
$B_{2g}(3)$	390		366	342
$B_{2g}(2)$	476		452	494
$B_{2g}(1)$	610		678	637
$B_{3g}(5)$	181	205	162	
$B_{3g}(3)$	288	284	303	
$B_{3g}(4)$	342	384		
$B_{3g}(2)$	413		485	
$B_{3g}(1)$	593		644	593

Table I: Calculated and experimentally obtained phonon modes of YMnO₃,[20] YTiO₃,[19] and the LTM phase of Y_{0.63}Ca_{0.37}TiO₃ measured at 10 K in $c(aa)\bar{c}$ geometry, respectively. The Raman shifts are given in units of cm^{-1} .

the modulation of the Ti-O bond distances, associated with orbital and charge ordering, are remarkably strong in these titanates,[15] which may explain the strong signal of the P3 feature as well as the strong temperature dependence.

Following the temperature evolution of P3 from room temperature to 10 K, the peak weight continuously increases and saturates between 100 K and 150 K, see Figure 4. Such a saturation behavior is also observed for the static G-type distortion pattern associated with the charge and orbital order of the LTM phase.[15] This similarity in saturation behavior indicates, that the $B_{2g}(1)$ modes become A_{1g} modes, which correspond to the static distortions of the LTM phase. As the unit cell volumes of LTO and LTM phases differ, strain plays an important role in the phase separated state, which has been reported in TEM measurements:[14] it has been observed that especially the LTO phase is highly strained in contrast to the LTM phase, which will favor phase separation.

The Raman spectra in the conducting domain show an abrupt change between 150 K and 180 K. This is especially seen in the peak weights of P1 and P2, shown as black and red curves in Figure 4 Both modes require a

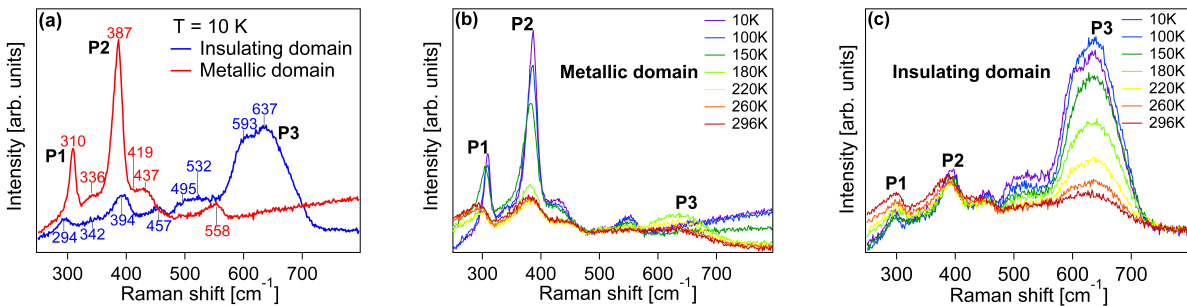


Figure 3: (Color online) (a) Raman scattering spectra of $Y_{0.63}Ca_{0.37}TiO_3$ single crystal, measured for dark and bright spots, shown in figure 1a, in $c(aa)\bar{c}$ geometry at 10 K. The spectrum in blue is obtained from a bright area, while the spectrum in red is obtained from a dark area. (b) and (c) temperature evolution of the Raman spectra of the dark and bright domains, respectively.

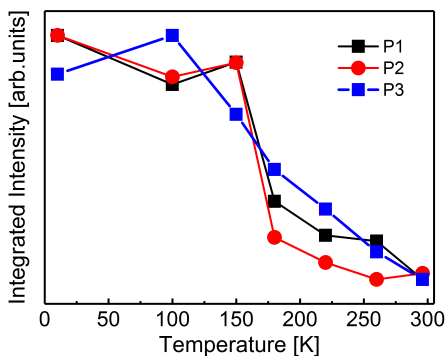


Figure 4: (Color online) Temperature evolution of the normalized integrated peak weights of the metallic (red and black) and insulating (blue) domains, represented by the peaks P1, P2, and P3, respectively.

description by an asymmetric Fano lineshape in the fits, which may hint to an enhanced coupling of the charge carriers to the phonon modes P1 and P2.

At room temperature, the spectra in the different regions of the material are almost identical, in agreement with the observation that in the microscope images the contrast between them is barely detectable.

IV. CONCLUSIONS

Combining our results from optical microscopy, spatially resolved photoelectron spectroscopy, and Raman scattering, we can identify regions of different crystallographic and, in turn, electronic character in the material, which form stripe-like domain patterns of typical sizes of order $20 \times 100 \mu m^2$. Along the direction of the stripes, these domains can extend up to several hundreds of μm . The result of our investigations of $Y_{0.63}Ca_{0.37}TiO_3$ allow us to assign the bright domains, see Figure 1a, to be insulating and the dark domains to be conducting by using Raman spectroscopy. The insulating domains are

furthermore identified with the LTM phase and the conducting domains with the LTO phase of the material. With these identifications, the optically observed percolation of the dark domains is indeed a percolation of the metallic LTO phase through the insulating LTM phase, which in the end leads to the macroscopic effect of a temperature-driven metal insulator transition. The domain patterns and the growth direction of the domains with varying temperature also explains the anisotropy observed in the resistivity.[19] As seen in the optical microscope pictures in Figure 1, the three differently oriented surfaces exhibit a preferred growth direction of the metallic domains in a- and c- directions. However the growth in b- direction is strongly suppressed. Resistivity measurements along a- and c- directions in the literature indeed show a temperature-driven metal to insulator transition, whereas in b- direction the MIT is strongly suppressed.[19] Different transition temperatures with varying stoichiometries ($x=0.37-0.39$) are reported in the literature.[11, 15] We attribute this to a faster percolation due to the higher number of metallic domains, and vice versa. In turn, the apparent natural inhomogeneity in the material is expected to result in spatially varying physical properties like transition temperatures. The reason for the stability of the insulating phase at high temperatures is still unclear and remains an open question.

In summary, we have performed microstructural measurements using optical microscopy, spontaneous micro-Raman scattering, and micro-photoemission on single crystals of $Y_{0.63}Ca_{0.37}TiO_3$ in a temperature range from 10 K to room temperature. We observe a phase separation throughout the temperature range and identify the structural and the electronic differences between the different domains as well as their temperature dependence. Our results suggest that the macroscopic change of the electronic transport behavior is a result of percolation of the conducting LTO phase inside a non conducting phase, which at high temperature has an orthorhombic crystal structure, but at low temperature becomes monoclinic.

V. ACKNOWLEDGMENTS

We gratefully acknowledge fruitful discussions with C. Schüßler-Langeheine and D. Khomskii. This work has

been supported by the Deutsche Forschungsgemeinschaft (DFG) through the Collaborative Research Center SFB 1238 (projects A02 and B03).

-
- [1] M. Imada, A. Fujimori, and Y. Tokura, *Rev. Mod. Phys.* **70**, 1039 (1998).
 - [2] C.-H. Yee, L. Balents, *Phys. Rev. X*, **5** 021007, (2015).
 - [3] Y. Cao, P. Shafer, X. Liu, D. Meyers, M. Kareev, S. Middey, J. W. Freeland, E. Arenholz, and J. Chakhalian, *Appl. Phys. Lett.* **107**, 112401 (2015).
 - [4] X. Yang and G. Wu, *EPL*, **117** 27004, (2017).
 - [5] T. Katsufuji, Y. Okimoto, and Y. Tokura, *Phys. Rev. Lett.* **75**, 3497 (1995).
 - [6] Y. Okimoto, T. Katsufuji, Y. Okada, T. Arima, and Y. Tokura, *Phys. Rev. B* **51**, 9581 (1995).
 - [7] K. Morikawa, T. Mizokawa, A. Fujimori, Y. Taguchi and Y. Tokura, *Phys. Rev. B* **54**, 8446 (1996).
 - [8] Y. Taguchi, Y. Tokura, T. Arima, and F. Inaba, *Phys. Rev. B* **48**, 511 (1993).
 - [9] Y. Tokura, Y. Taguchi, Y. Moritomo, K. Kumagai, T. Suzuki, and Y. Iye, *Phys. Rev. B* **48**, 14063 (1993).
 - [10] F. Iga, T. Naka, T. Matsumoto, N. Shirakawa, K. Murata, and Y. Nishihara, *Physica B* **223 & 224**, 526-528 (1996).
 - [11] K. Kato, E. Nishibori, M. Takata, M. Sakata, T. Nakano, K. Uchihira, M. Tsubota, F. Iga, and T. Takabatake, *J. Phys. Soc. Japan* **71**, 2082 (2002).
 - [12] H. Nakao, M. Tsubota, F. Iga, K. Uchihira, T. Nakano, T. Takabatake, K. Kato, and Y. Murakami, *J. Phys. Soc. Japan* **73**, 2620 (2004).
 - [13] M. Tsubota, F. Iga, T. Nakano, K. Uchihira, S. Kura, M. Takemura, Y. Bando, K. Umeo, T. Takabatake, E. Nishibori, M. Takata, M. Sakata, K. Kato, and Y. Ohishi, *J. Phys. Soc. Japan* **72**, 3182 (2003).
 - [14] H. Matsuhata, F. Iga, M. Tsubota, T. Nakano, T. Takabatake, and K. Kato, *Phys. Rev. B* **70**, 134109 (2004).
 - [15] A. C. Komarek, Dissertation, Univ. Cologne (2009), <https://kups.ub.uni-koeln.de/2982/>
 - [16] M. Tsubota, F. Iga, K. Uchihira, T. Nakano, S. Kura, M. Takabatake, S. Kodoma, H. Nakao, and Y. Murakami, *J. Phys. Soc. Jpn.* **74**, 12, 3259-3266 (2005)
 - [17] F. Barbo, M. Bertolo, A. Bianco, G. Cautero, S. Fontana, T.K. Johal, S. La Rosa, K. Kaznatcheyev, and G. Margaritondo, *Rev. Sci. Instrum.* **71**, 1 (2000).
 - [18] T. Katsufuji and Y. Tokura, *Phys. Rev. B* **50**, 2704 (1994).
 - [19] T. Tsurui, N. Ogita, M. Udagawa, M. Tsubota, and F. Iga, *Phys. Rev. B* **69**, 024102 (2004).
 - [20] M. N. Iliev, M. V. Abrashev, H.-G. Lee, V. N. Popov, Y. Y. Sun, C. Thomsen, R. L. Meng, and C. W. Chu, *Phys. Rev. B* **57**, 2872 (1998).